Simulation of the beam-beam effects in e^+e^- storage rings with a method of reduced region of mesh

Yunhai Cai, Alex W. Chao, and Stephan I. Tzenov
Stanford Linear Accelerator Center, Stanford University, Stanford, California 94309

Toshi Tajima
University of Texas at Austin, Austin, Texas 78712
and Lawrence Livermore National Laboratory, Livermore, California 94551

(Received 30 August 2000; revised manuscript received 22 December 2000; published 18 January 2001)

A highly accurate self-consistent particle code to simulate the beam-beam collision in e^+e^- storage rings has been developed. It adopts a method of solving the Poisson equation with an open boundary. The method consists of two steps: assigning the potential on a finite boundary using Green's function and then solving the potential inside the boundary with a fast Poisson solver. Since the solution of Poisson's equation is unique, our solution is exactly the same as the one obtained by simply using Green's function. The method allows us to select a much smaller region of mesh and therefore increase the resolution of the solver. The better resolution makes more accurate the calculation of the dynamics in the core of the beams. The luminosity simulated with this method agrees quantitatively with the measurement for the PEP-II B Factory ring in the linear and nonlinear beam current regimes, demonstrating its predictive capability in detail.

DOI: 10.1103/PhysRevSTAB.4.011001 PACS numbers: 29.27.Bd, 29.20.Dh, 29.27.Eg, 29.27.Fh

I. INTRODUCTION

The beam-beam interaction is one of the most important limiting factors determining the luminosity of storage colliders. It has been studied extensively by theoretical analysis [1], experimental measurements [2], and computer simulations [3]. Historically, due to the complexity of the interaction, many approximations, such as strong-weak [4] or soft-Gaussian [5], have been introduced in order to simulate the interaction in a reasonable computing time. The self-consistent simulation of the beam-beam interaction by solving the Poisson equation with a boundary condition has been proposed to investigate first the round beams [6] and then the flat beams [7]. To enhance the accuracy and reduce the computational overhead, an algorithm (and a code) of the so-called δf method that can handle strong-strong interactions has been introduced [8]. Another self-consistent approach to the beam-beam interaction is to use Green's function directly or indirectly [9,10].

In the present paper we will develop a method that takes advantages from both self-consistent approaches: a smaller region of mesh from the method of using Green's function and a faster solver for the interior. In order to develop a highly accurate predictive code at the luminosity saturation region, it is necessary to have a fully self-consistent treatment of the field-particle interaction at collision. Since we are interested in simulating the asymmetric e^+e^- storage collider PEP-II [11], which needs to maximize the luminosity and thus the beam current, it is even more crucial that the beam-beam interaction in the large current regime be treated accurately.

In a self-consistent simulation of the beam-beam interaction in storage rings, the beam distributions have to be evolved dynamically during collision with the opposing beam together with the propagation in the rings. During collision, the beam distributions are used at each time sequence to compute the force that acts on the opposing beam.

Since positrons and electrons are ultrarelativistic particles in high-energy storage rings, the beam-beam force is transverse and acts only on the opposing beam. Hence, given a beam distribution, we can divide the distribution longitudinally into several slices and then solve for the two-dimensional force for each slice. Self-consistency is achieved by introducing many-body particles in the field that in turn constitute charge current, the strategy of the particle-in-cell (PIC) procedure (see, for example, Ref. [12]). In this paper, for simplicity, we use only a single longitudinal slice for a bunch, ignoring any beam-beam effects encompassing over the length of the bunch.

II. METHOD

In modern colliders, beams are focused strongly at the interaction point to achieve high luminosity. As a result, the transverse dimension of the beam is much smaller than the dimension of the beam pipe at the collision point. Therefore, the open boundary condition is a good approximation for calculating the transverse beam-beam force.

A. Green's function

Given a charge density $\rho_c(x, y)$, which is normalized to the total charge

$$\int dx\, dy\, \rho_c(x,y) = Ne\,, \tag{2.1}$$

where N is the total number of particles, the electric potential $\phi(x,y)$ satisfies the Poisson equation

$$\left(\frac{\partial^2}{\partial x^2} + \frac{\partial^2}{\partial y^2}\right)\phi(x,y) = -2\pi\rho_c(x,y)\,, \tag{2.2}$$

with x and y being the transverse coordinates. The solution of the Poisson equation can be expressed as

$$\phi(x,y) = \int dx'\, dy'\, G(x - x', y - y')\rho_c(x',y')\,, \tag{2.3}$$

where G is Green's function which satisfies the equation

$$\left(\frac{\partial^2}{\partial x^2} + \frac{\partial^2}{\partial y^2}\right)G(x - x', y - y') = -2\pi\delta(x - x')\delta(y - y')\,. \tag{2.4}$$

In the case of open boundary condition, namely the boundary is far away so that its contribution to the potential can be ignored, one has the well-known explicit solution for Green's function:

$$G(x - x', y - y') = -\frac{1}{2}\ln[(x - x')^2 + (y - y')^2]. \tag{2.5}$$

This explicit solution can be used directly to compute the potential. The main problem of this approach is that it is slow to calculate the logarithm and the number of computations is proportional to the square of the number of macroparticles N_p^2. One can reduce N_p by introducing a two-dimensional mesh to smooth out the charge distribution [9]. Or to further improve the computing speed, one can map the solution onto the space of spectrum by the fast Fourier transformation (FFT) and then calculate the potential [9,10].

B. Reducing the region of mesh

Another alternative approach is to solve the Poisson equation with a boundary condition [7], because the region (20 μm $\times$ 450 μm for PEP-II) occupied by the beam is much smaller than the boundary defined by the beam pipe (2 cm radius) at the collision point. In order to achieve required resolution, a few mesh points per σ of the beam are needed, otherwise the size of mesh is too large for numerical computation.

However, it is unnecessary to cover the entire area with mesh inside the beam pipe since the area is mostly empty. We chose a smaller and finite area of the mesh, which is large enough to cover the whole beam, and, by carefully selecting the potential on the boundary, we can obtain the accurate solution inside the boundary.

We denote by ϕ_1 the solution (2.3) of the Poisson equation. Let ϕ_2 be the solution obtained by solving the Poisson equation in a two-dimensional area S with the potential prescribed on a closed one-dimensional L bounding the area S,

$$\phi_2(x,y) = \int_S dx'\, dy'\, G(x - x', y - y')\rho_c(x',y')\,, \tag{2.6}$$

where $(x,y) \in L$. By definition, we have $\phi_1 = \phi_2$ on the boundary L. Let $U = \phi_1 - \phi_2$ and use the first identity of Green's theorem [13] in two dimensions,

$$\int_S [U\nabla^2 U + (\nabla U)^2]\, dx\, dy = \oint_L U\,\frac{\partial U}{\partial n}\, dl\,, \tag{2.7}$$

where dl is a line element of L with a unit outward normal n. Since $U = 0$ on L and $\nabla^2 U = 0$ inside L, we have

$$\int_S (\nabla U)^2\, dx\, dy = 0\,, \tag{2.8}$$

implying that U is a constant inside L. We can set $U = 0$, which is consistent with the value on the boundary. Hence, $\phi_1 = \phi_2$. The two solutions are identical.

III. FIELD SOLVER

We adopt the PIC technique to calculate the fields induced by the charge (and current) of the beams self-consistently. The charge distribution of a beam is represented by macroparticles. These macroparticles are treated as a single electron or positron dynamically. In order to compute the field acting on the particles of the opposing beam, we first deposit their charges onto the grid points of a two-dimensional rectangular mesh. We denote by H_x the horizontal distance between two adjacent grid points and by H_y the distance in vertical direction.

A. Charge assignment

We chose the method of the triangular-shaped cloud [14] as our scheme for the charge assignment onto the grid. On a two-dimensional grid, associated with each macroparticle, nine nearest points are assigned with nonvanishing weights as illustrated in Fig. 1. We use "0" to denote the first, "+" as the second, and "−" as the third nearest lines.

The weights are quadratic polynomials of the fractional distance, $r_x = \delta x/H_x$, to the nearest line

$$\begin{aligned} w_x^0 &= \frac{3}{4} - r_x^2\,, \\ w_x^+ &= \frac{1}{2}\left(\frac{1}{4} + r_x + r_x^2\right), \\ w_x^- &= \frac{1}{2}\left(\frac{1}{4} - r_x + r_x^2\right). \end{aligned} \tag{3.1}$$

The coefficients are chosen such that the transition at the middle of the grid is continuous and smooth, and $w_x^0 + w_x^+ + w_x^- = 1$, which is required by the conservation of charge. In order to retain these properties, the weights of the two-dimensional grid are simply a product of two

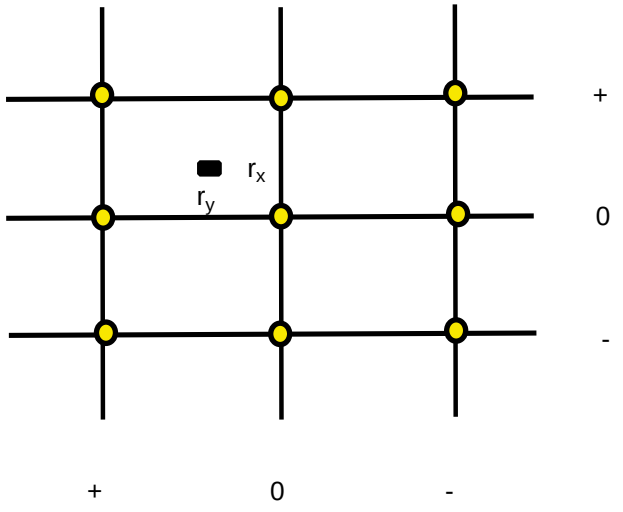

FIG. 1. (Color) Scheme of charge assignment.

one-dimensional weights. For example, $w^{00} = w_x^0 w_y^0$ or $w^{+-} = w_x^+ w_y^-$.

B. Poisson solver

It is crucial to solve the Poisson equation fast enough (within a second on a computer workstation) for the beam-beam simulation, because the radiation damping time is about 5000 turns and several damping times are needed to reach an equilibrium distribution. For the reason of the computing speed, we follow Krishnagopal [7] and choose the method of cyclic reduction and FFT [15]. A five-point difference scheme is used to approximate the two-dimensional Laplacian operator

$$\frac{\phi_{i-1,j} + \phi_{i+1,j} - 2\phi_{i,j}}{H_x^2} + \frac{\phi_{i,j-1} + \phi_{i,j+1} - 2\phi_{i,j}}{H_y^2} = -2\pi\rho_{ci,j}\,, \tag{3.2}$$

where i and j are the horizontal and vertical indices that label the grid points on the mesh.

Truncation errors are of the order of H_x^2 and H_y^2. It is worthwhile to mention that, if we use the same number of mesh points per σ in both transverse directions in the case of beam aspect ratio 30:1, the truncation errors in the horizontal plane are dominant. To minimize the errors in our simulation, we select 3 times more mesh points per σ in the horizontal direction compared to the vertical one.

C. Field

The field $\vec{E} = -\nabla\phi$ is computed on the two-dimensional grid, using a six-point difference scheme

$$E_{xi,j} = -\frac{1}{12H_x}[(\phi_{i+1,j+1} - \phi_{i-1,j+1}) + 4(\phi_{i+1,j} - \phi_{i-1,j}) + (\phi_{i+1,j-1} - \phi_{i-1,j-1})], \tag{3.3}$$

$$E_{yi,j} = -\frac{1}{12H_y}[(\phi_{i+1,j+1} - \phi_{i+1,j-1}) + 4(\phi_{i,j+1} - \phi_{i,j-1}) + (\phi_{i-1,j+1} - \phi_{i-1,j-1})]. \tag{3.4}$$

The field off the grid is computed with the same smoothing scheme used in the charge assignment to ensure the conservation of momentum. The fields E_x and E_y are interpolated between the grid points. They are calculated by using the weighted summation of the fields at the nine nearest points with exactly the same weights used as the charge is assigned.

IV. PARTICLE TRACKING

The motion of a particle is described by its canonical coordinates

$$z^T = (x, P_x, y, P_y)\,, \tag{4.1}$$

where P_x and P_y are particle momenta normalized by the design momentum p_0.

A. One-turn map

When synchrotron radiation is turned off, a matrix is used to describe the linear motion in the lattice

$$z_{n+1} = M z_n\,, \tag{4.2}$$

where M is a 4×4 symplectic matrix which can be partitioned into blocks of 2×2 matrices when linear coupling is ignored,

$$M = \begin{pmatrix} M_x & 0 \\ 0 & M_y \end{pmatrix}. \tag{4.3}$$

Here M_x and M_y are 2×2 symplectic matrices. The matrix M_x is expressed with the Courant-Snyder parameters β_x, α_x, and γ_x at the collision point,

$$M_x = \begin{pmatrix} \cos(2\pi\nu_x) + \alpha_x \sin(2\pi\nu_x) & \beta_x \sin(2\pi\nu_x) \\ -\gamma_x \sin(2\pi\nu_x) & \cos(2\pi\nu_x) - \alpha_x \sin(2\pi\nu_x) \end{pmatrix}, \tag{4.4}$$

where ν_x is the horizontal tune. A similar expression is applied in the vertical plane.

B. Damping and synchrotron radiation

Following Hirata [16], we apply the radiation damping and quantum excitation in the normalized coordinates, since it is easily generalized to include linear coupling. The motion of a particle in the normalized coordinates is described by a rotation matrix

$$R_x = \begin{pmatrix} \cos(2\pi\nu_x) & \sin(2\pi\nu_x) \\ -\sin(2\pi\nu_x) & \cos(2\pi\nu_x) \end{pmatrix}, \tag{4.5}$$

which is obtained by performing the similarity transformation

$$R_x = A_x^{-1} M_x A_x \,, \tag{4.6}$$

where

$$\begin{aligned} A_x &= \begin{pmatrix} \sqrt{\beta_x} & 0 \\ -\frac{\alpha_x}{\sqrt{\beta_x}} & \frac{1}{\sqrt{\beta_x}} \end{pmatrix}, \\ A_x^{-1} &= \begin{pmatrix} \frac{1}{\sqrt{\beta_x}} & 0 \\ \frac{\alpha_x}{\sqrt{\beta_x}} & \sqrt{\beta_x} \end{pmatrix}. \end{aligned} \tag{4.7}$$

When synchrotron radiation is switched on, we simply replace the rotation matrix R_x with the following map in the normalized coordinates $\bar{x}$ and $\bar{P}_x$,

$$\begin{pmatrix} \bar{x} \\ \bar{P}_x \end{pmatrix} = e^{-1/\tau_x} R_x \begin{pmatrix} \bar{x} \\ \bar{P}_x \end{pmatrix} + \sqrt{\epsilon_x (1 - e^{-2/\tau_x})} \begin{pmatrix} \eta_{\bar{x}} \\ \eta_{\bar{P}_x} \end{pmatrix}, \tag{4.8}$$

where $\eta_{\bar{x}}$ and $\eta_{\bar{p}_x}$ are Gaussian random variables normalized to unity, τ_x is the damping time in units of the number of turns, and ϵ_x is the equilibrium emittance. In the vertical plane, a similar map is applied.

C. Beam-beam kick

Assuming particles are ultrarelativistic and the collision is head-on, the kick on a particle by the opposing beam is given by the Lorenz force

$$\delta P_x = -\frac{2e}{E_0} E_x \,, \tag{4.9}$$

$$\delta P_y = -\frac{2e}{E_0} E_y \,, \tag{4.10}$$

where E_x and E_y are the horizontal and vertical components of the electric field evaluated at the position of the particle. They are computed with the Poisson solver as outlined in the previous section each time two slices of the beam pass each other. Half of the transverse force is the magnetic force due to the beam moving at the speed of light. The energy of the particle $E_0 = cp_0$, appearing in the denominator of the above expressions, comes from the normalization of the canonical momenta P_x and P_y and the use of the s coordinate $s = ct$ as the "time" variable.

A typical beam-beam kick experienced by a particle near the axis is shown in Fig. 2 with the PEP-II parameters, which are tabulated in the next section. As expected based on the derivation in Sec. II B, the kick that resulted from solving the Poisson equation with the inhomogeneous boundary condition agrees well with the analytic solution. In addition, the agreement demonstrates that the scheme of the charge deposition works well, the mesh is dense enough, and the number of macroparticles is large enough.

The number of macroparticles used to represent the distribution of the beam is 10 240. The area of the mesh is $8\sigma_x \times 24\sigma_y$, and there are 15 grid points per σ_x and five per σ_y. There are about 15 macroparticles per cell within 3σ of the beam. These parameters are chosen to

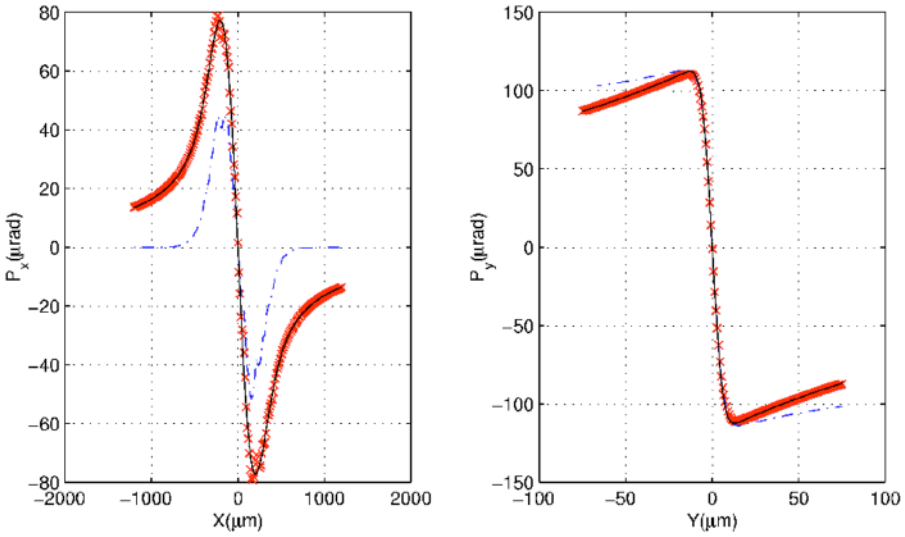

FIG. 2. (Color) The beam-beam kick by a flat Gaussian beam with aspect ratio 30:1 near the x and y axes. The dash-dotted curve is the case when $\phi = 0$ is assigned as the boundary condition. The "×" is the kick when the inhomogeneous boundary condition is used. The solid curve is the kick produced by the Erskine-Bassetti formula [17].

minimize truncation errors and maximize resolution. The 256×256 mesh is also the maximum allowed by a computer workstation to complete a typical job within a reasonable time.

The discrepancy between the solution with the homogeneous boundary condition $\phi = 0$ and the analytic one worsens as the beam aspect ratio becomes larger because the actual change of the potential on the horizontal boundaries becomes larger.

V. APPLICATION TO PEP-II

An object-oriented C++ class library has been written to simulate the beam-beam interaction using the method outlined in the previous sections. In the library, the beam and the Poisson solver are all independent objects that can be constructed by the user. For example, there is no limitation on how many objects of the beam are allowed in the simulation, and the beams can have different parameters as an instance of the beam class. These features provide us with great flexibility to study various phenomena of the beam-beam interaction.

We will carry out the simulation of beam-beam interaction with the current operating parameters of the PEP-II so that the results of the simulation can be compared with the known experimental observations. As a goal of this study, after a proper benchmarking of the code against the experiment, we shall be able to make predictions on parameter dependence and show how to improve the luminosity performance of the collider.

A. PEP-II operating parameters

The parameters used in the simulation are tabulated in Table I. The vertical β_y^* at the interaction point (IP) is lowered to 1.25 cm [18] from the design value 1.5 cm [11]. The horizontal emittance 24 nm rad in the low energy ring (LER) is one-half of the design value 48 nm rad because the wiggler has been turned off to increase the luminosity. The damping time, 9740 turns, in the LER is a factor of 2 larger than the one in the high energy ring (HER) because of the change of the wigglers made during the construction of the machine. The degradation of luminosity from the increase of the damping time was then found to be about 10% based on the beam-beam simulation. The tunes are split and are determined experimentally to optimize the peak luminosity.

TABLE I. Parameters for the beam-beam simulation.

Parameter	Description	LER (e^+)	HER (e^-)
E (GeV)	Beam energy	3.1	9.0
β_x^* (cm)	Beta X at the IP	50.0	50.0
β_y^* (cm)	Beta Y at the IP	1.25	1.25
τ_t (turn)	Transverse damping time	9740	5014
ϵ_x (nm rad)	Emittance X	24.0	48.0
ϵ_y (nm rad)	Emittance Y	1.50	1.50
ν_x	X tune	0.649	0.569
ν_y	Y tune	0.564	0.639

B. Procedure of simulation

The distribution of the beam is represented as a collection of macroparticles that are dynamically tracked. The procedure to obtain equilibrium distributions of the two colliding beams is as follows: (i) initialize the four-dimensional Gaussian distribution according to the parameters of the lattice at the collision point and the emittance of the beam. The distributions of two beams are independent and different; (ii) iterate a loop with three damping times; (iii) propagate each beam through the corresponding lattice using a one-turn map with synchrotron radiation; (iv) cast the particle distributions onto the grid as the charge distribution with weighting and smoothing; (v) solve for the potential on the grid with the Poisson solver; (vi) compute the field on the grid; (vii) calculate the beam-beam kick to the particles of the other beam with the field at the position of the particles. The field off the grid is interpolated with the same weighting and smoothing used in the charge deposition; (viii) save data such as beam size, beam centroid, and luminosity; (ix) end of the loop; (x) save the final distributions.

We vary the beam intensity with a step of $\delta N^+ = 10^{10}$ and the fixed beam current ratio I_+:I_- = 2:1, which is close to the ratio for the PEP-II operation. At each beam current, we compute the equilibrium distributions.

Particle loss outside the area ($8\sigma_x \times 24\sigma_y$) covered by the mesh is closely monitored. There is no loss at the low beam currents (the first 15 data points). At very high current (beyond the 15th data point), the loss is still less than 1%.

C. Beam-beam blowup

Given equilibrium distributions that are close enough to the Gaussian, we can introduce the beam-beam parameters

$$\xi_x^{\pm} = \frac{r_e N^{\mp} \beta_x^{\pm}}{2\pi\gamma^{\pm}\sigma_x^{\mp}(\sigma_x^{\mp} + \sigma_y^{\mp})}, \qquad \xi_y^{\pm} = \frac{r_e N^{\mp} \beta_y^{\pm}}{2\pi\gamma^{\pm}\sigma_y^{\mp}(\sigma_x^{\mp} + \sigma_y^{\mp})}, \tag{5.1}$$

where r_e is the classical electron radius, γ is the energy of the beam in units of the rest energy, and N is the total number of the charge in the bunch. Here the superscript "+" denotes quantities corresponding to the positron beam and "−" denotes quantities corresponding to the electron beam.

The results of the simulation are summarized in Fig. 3. The horizontal size of the positron beam grows linearly as the currents increase while the horizontal size of the electron beam remains unchanged. We see that the reduction of the horizontal size of the positron beam at the low current

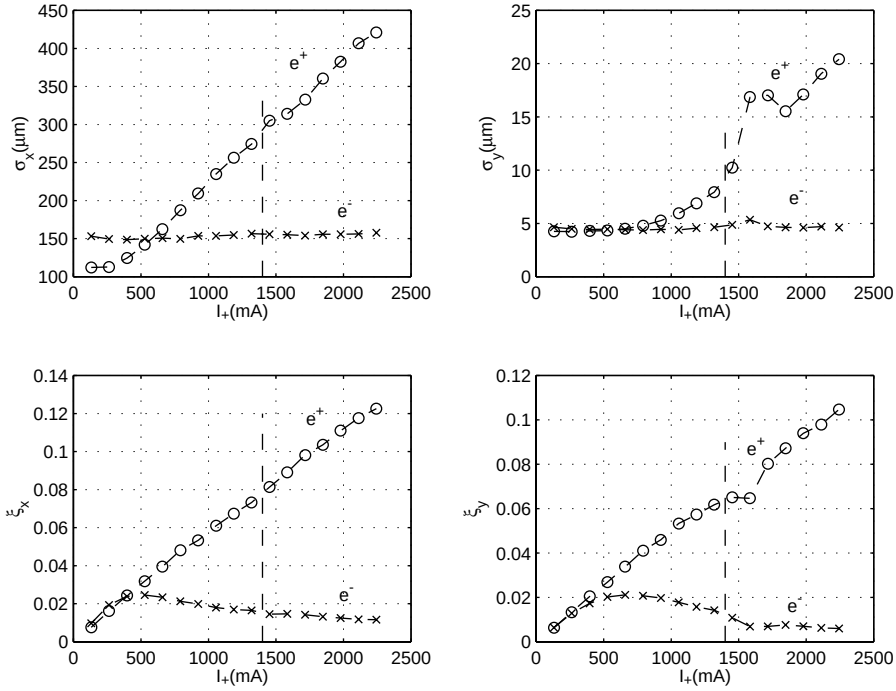

FIG. 3. The beam size and beam-beam tune shifts as a function of the positron current while the electron current is fixed at one-half of the positron current. The dashed line presents the maximum operating current of the positron beam with 605 bunches at 1400 mA.

has helped to match its beam size to the horizontal size of the electron beam. That is the reason that turning off the wiggler in the LER has helped to increase the luminosity.

In the vertical plane, the beam sizes are reasonably matched until $I_+ = 1000$ mA. The final vertical blowup of the positron beam near $I_+ = 1400$ mA is the cause of the saturated luminosity. The large vertical mismatch at the higher current could also lead to the deterioration of the beam lifetime during the collision. As a result, the maximum current of the positron beam is limited to below 1400 mA.

Experimentally, there is no blowup of beam size in either plane seen in the electron beam. For the positron beam, the sizes in both planes grow as the currents increase. However, it is difficult at this point to make quantitative comparisons between measurement and simulation because the resolution of the synchrotron monitors is unknown, particularly due to the heating damage when they were installed.

As shown in the figure, at the maximum operating currents $I_+ = 1400$ mA and $I_- = 700$ mA, the vertical beam-beam tune shifts for positrons are about 0.06 and for electrons 0.015. The large differences in the tune shifts are a direct consequence of the mismatch of the beam sizes and the violation of the energy transparency condition $I_+\gamma_+ = I_-\gamma_-$. The lower current ratio makes the positron beam weaker and the electron beam stronger. It is clear that the positron beam is weaker than the electron beam at this working point and current ratio.

D. Luminosity

Given the two beam distributions, ρ^+ and ρ^-, the luminosity can be written as

$$L = n_b f_0 N^+ N^- \int_{-\infty}^{\infty}\int_{-\infty}^{\infty} \rho^+(x,y)\rho^-(x,y)\,dx\,dy\,, \tag{5.2}$$

where n_b is the number of the colliding bunches, f_0 is the revolution frequency, and N^+, N^- are the number of particles in each position and electron bunch, respectively. Since the distribution ρ is normalized to unity

$$\int dx\,dy\,\rho(x,y) = 1 \tag{5.3}$$

and proportional to the charge density ρ_c, we evaluate the overlapping integral by a summation over $\rho_c^+\rho_c^-$ on the mesh. Furthermore, if we assume the distributions are Gaussian, the overlapping integral can be carried out,

$$L = \frac{n_b f_0 N^+ N^-}{2\pi\Sigma_x\Sigma_y}\,, \tag{5.4}$$

where $\Sigma_x = \sqrt{\sigma_x^{+2} + \sigma_x^{-2}}$ and $\Sigma_y = \sqrt{\sigma_y^{+2} + \sigma_y^{-2}}$. The two methods agree within a few percent. The mesh method gives a higher luminosity than the Gaussian one. We always use the mesh method, since it can be applied to broad classes of distribution.

The luminosity as a function of beam current is shown in Fig. 4. The maximum luminosity with a different number of bunches is corresponding to n_b times of the saturated

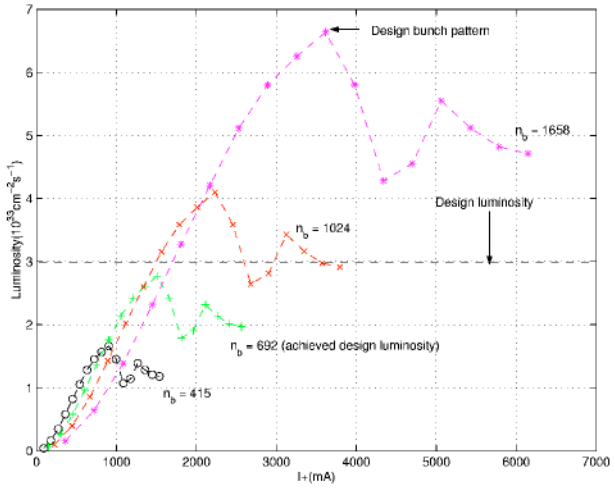

FIG. 4. (Color) Luminosity as a function of the beam current. The labels are the number of the colliding bunches.

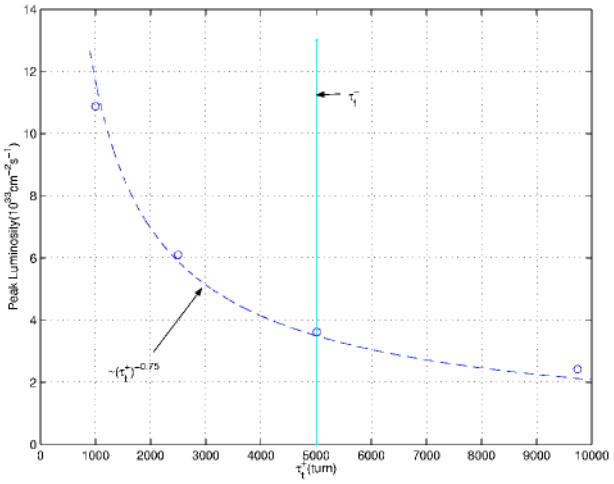

FIG. 5. (Color) Peak luminosity affected by the damping time of the LER with 605 bunches. The circles represent the simulation result and the dashed line represents the fitted curve of $2081(\tau_t^+)^{-0.75}$.

TABLE II. Luminosity comparisons for PEP-II.

Month	n_b	L_{meas}	L_{sim}
May	554	1.90	2.20
August	605	2.20	2.40
October	692	3.10	2.80

luminosity of a single bunch. The single bunch luminosity is limited by a final rapid vertical blowup of the positron beam, as discussed in the previous section. In the accelerators, the number of bunches is limited by the electron-cloud instability [19] in the LER. We expect that, as the effects of electron-cloud reduce while more solenoids are added into the ring, the maximum luminosity should increase as the number of bunches increase according to the figure. As tabulated in Table II, the result of the simulation has been reasonably followed since April, 2000, after which the configuration of the machines was kept fixed to the values listed in Table I.

The luminosity tabulated in the table is in the unit of 10^{33} cm^{-2} s^{-1}. Note that the ratio of beam currents I_+:I_- actually used in the operations is not always exactly 2:1 as used in the simulation. For example, when the design luminosity was reached, $I_+ = 1550$ mA and $I_- = 800$ mA.

If this trend continues, the luminosity allowed by the beam-beam interaction with the design bunch pattern (1658 bunches) should reach 6.5×10^{33} cm^{-2} s^{-1} with $I_+ = 3500$ mA and $I_- = 1750$ mA, unless longitudinal effects such as the hourglass effect set in earlier than we presently expect.

E. Damping time

Historically, the damping time is typically not considered to be an important parameter for the beam-beam effects. For this reason we make an attempt to reduce the damping time artificially for the LER to speed up the computation. The result is shown in Fig. 5.

The only difference of the parameters used in the simulation is the damping time in the LER. In particular, the damping time of the HER is fixed at $\tau_t^- = 5014$. Indeed, at low currents, the difference of the luminosity is rather small, which is consistent with the simulation performed when the change of the wiggler was made. But the difference grows larger as the current increases. Near the peak luminosity for the PEP-II operation $I_+ = 1400$ mA, the luminosity difference between $\tau_t^+ = 5014$ and $\tau_t^+ = 9740$ is about 40% according to Fig. 5, which is significant.

This result shows for the first time that the damping time is a rather important parameter for the computation of the peak luminosity at high beam currents. Secondly, it points out a way to improve the peak luminosity of the PEP-II without the increase of the beam currents, namely, to install another wiggler in the LER to reduce the damping time to the original design value.

F. Routine operation

To make a direct comparison between simulation and experimental observation, we have recorded the luminosity during a typical delivering operation of PEP-II. The data in a period of 2 h on September 15, 2000 are shown in Fig. 6. The duration of each measurement was 3 min. The first and second plots in the figure present the total decaying beam current of positron and electron beams, respectively. The third plot shows the measured luminosity and simulated luminosity at the same beam current displayed in the figure. The other parameters used in the simulation are the same as in Table I. At these beam intensities, there are no lost particles in the simulation.

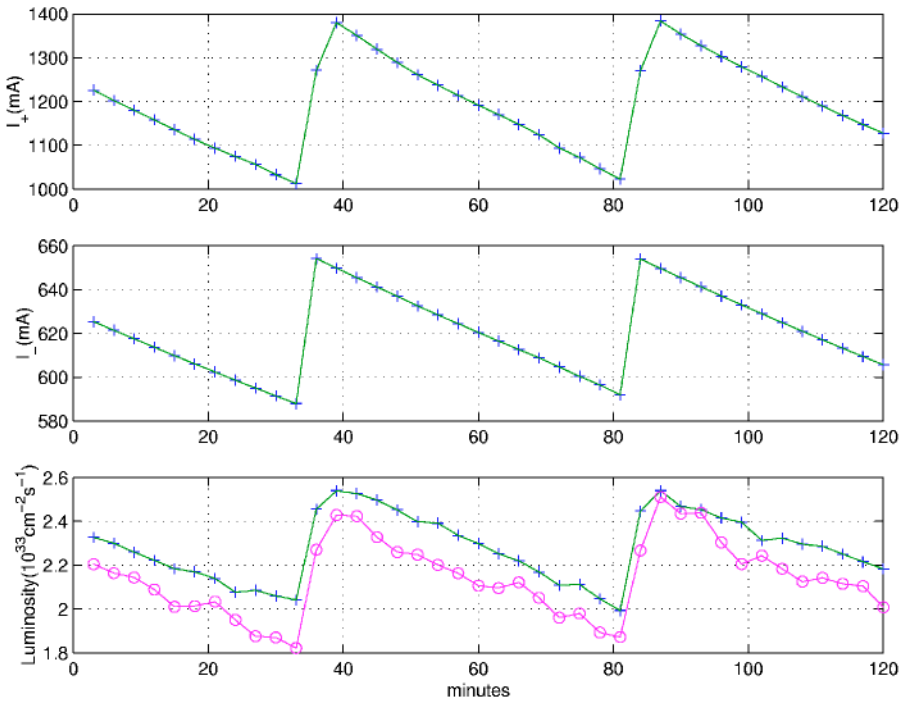

FIG. 6. (Color) Luminosity of a routine operation of PEP-II. The crosses represent measurement and the circles represent simulation. The number of bunches was 605.

The agreement of the simulation and measurement was within 10%, and the simulated luminosity was actually lower than the measured one. Since the longitudinal effects of the beam-beam interaction are not yet included in the simulations, three-dimensional simulation could reduce further the simulated luminosity. For example, the hourglass effect should reduce the simulated luminosity by 12% given $\sigma_z = 1.3$ cm and $\beta_y^* = 1.25$ cm.

The disagreement between the measurement and the simulation reflects also the uncertainty of those parameters relevant to the beam-beam interaction. For instance, the β functions are known to within only about 10% in the machines. The fact that the measured luminosity is larger than the simulated one could be a consequence of the tuning bias toward the highest luminosity within the boundary of the parameters when the machines are tweaked by the operators.

VI. COLLECTIVE BEAM-BEAM EFFECTS

It was shown in the previous section that the beam-beam simulations of the PEP-II with an aspect ratio 30:1 agrees with the experimental measurements at about the 10% level. As in many cases, it is difficult to know exactly the causes of the difference between simulation and measurement since the real machines are often much more complicated than the simple model used in the simulation. As a useful and practical method, it is very important to first make sure that the simulation results are correct given the input parameters and then to find which input parameters describe the real machines.

We have shown that the beam-beam kick given by a Gaussian beam using this method of mesh reduction agrees well with the analytical solution. To check dynamics effects of the beam-beam interaction, we chose to simulate the effects of coherent resonance because they are more stringent and distinctive phenomena. As we know, Krishnagopal and Siemann [6] have found period-n solutions due to the collective beam-beam interaction near the tune of 0.79. We made two simulations with the parameters tabulated in Table III. These parameters give an aspect ratio of 8:1 and are the same as those used by Krishnagopal [20].

The results of the simulation are shown in Fig. 7. They are essentially the same as the published results using the

TABLE III. Parameters for the coherent resonance.

Parameter	Description	LER (e^+)	HER (e^-)
E (GeV)	Beam energy	3.1 or 3.0	9.0
β_x^* (cm)	Beta X at the IP	12.0	12.0
β_y^* (cm)	Beta Y at the IP	1.50	1.50
τ_t (turn)	Transverse damping time	1000	1000
ϵ_x (nm rad)	Emittance X	50.0	50.0
ϵ_y (nm rad)	Emittance Y	6.25	6.25
ν_x	X tune	0.79	0.79
ν_y	Y tune	0.79	0.79
I (mA)	Bunch current	6.0	2.0

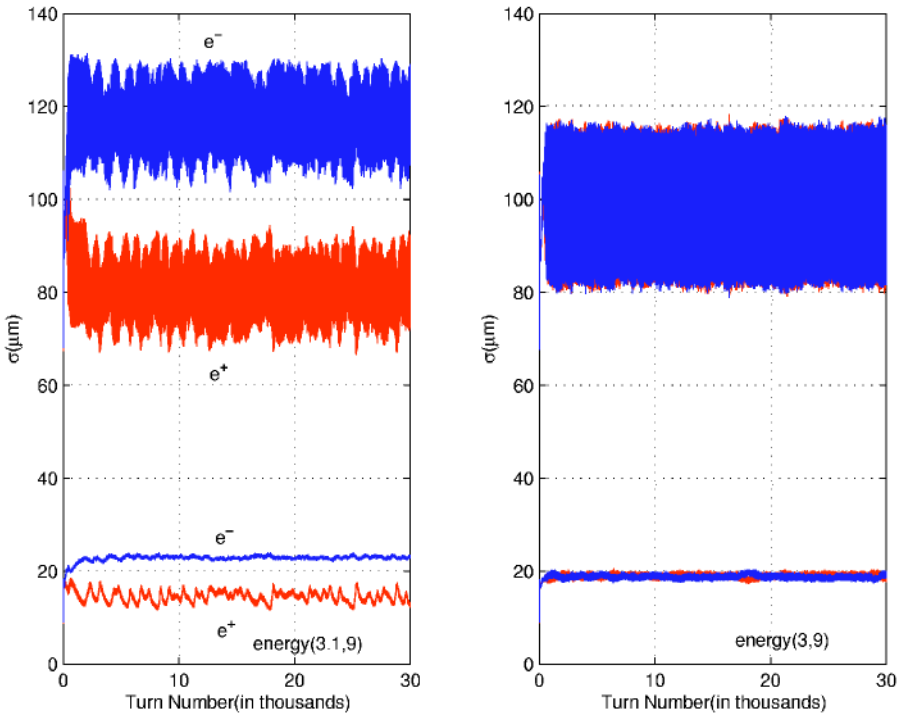

FIG. 7. (Color) Beam size vs turn number. As shown in the left-hand plot, a flip-flop solution is found with $E_+ = 3.1$ GeV and $E_- = 9.0$ GeV when the energy transparency condition is violated, and in the right-hand plot the period-3 solution [6] is found with $E_+ = 3.0$ GeV and $E_- = 9.0$ GeV when the energy transparency condition is preserved.

code CBI [20]. The small differences in the flip-flop solution are probably due to the different smoothing schemes used in the codes. These simulations make a benchmark against one of the existing codes under the same set of parameters and conditions.

VII. DISCUSSION

We have developed a hybrid method of solving the potential with an open boundary by using Green's function to fix the potential on a finite boundary and then to solve the Poisson equation for the potential inside the boundary. The method is applied to the simulation of strong-strong interaction of beam-beam effects in PEP-II. The preliminary results of this simulation show a very good quantitative agreement with the experimental observations. Given the simplicity of the two-dimensional model used, the achievement is surprising and remarkable. We have demonstrated that the present code has a highly reliable predictive capability of realistic beam-beam interaction. To further benchmark the code, we need to extend the simulation to include the finite length of the bunch and compare the simulation results directly to controlled experiments.

This method is quite general. It can be applied to the problem of space charge in three dimensions. It can also be used in the beam-beam interaction of a linear collider, aside from the additional bremsstrahlung effects. Finally, it can be applied to any boundary condition to reduce the region of the mesh if Green's function is known.

ACKNOWLEDGMENTS

We would like to thank John Irwin, John Seeman, and Ron Ruth for their continuous support and encouragement. We would like also to thank Franz-Josef Decker, Miguel Furman, Sam Heifets, Albert Hoffmann, Witold Kozanecki, Michiko Minty, Robert Siemann, Mike Sullivan, Robert Warnock, Uli Wienands, and Yiton Yan for helpful discussions. Especially, we would like to thank Srinvas Krishnagopal for many explanations of the PIC method during his visit at SLAC. This work was supported by the U.S. Department of Energy under Contracts No. DE-AC03-76SF00515, No. W-7405-Eng.48, and No. DE-FG03-96ER40954.

[1] See, for example, A. W. Chao, P. Bambade, and W. T. Weng, in *Proceedings of the US-CERN School on Particle Accelerators, Santa Margherita di Pula, Sardinia, 1985,* edited by J. M. Jowett, M. Month, and S. Turner, Lecture Notes in Physics, Vol. 247 (Springer-Verlag, Berlin, 1986), p. 77.

[2] See, for example, J. T. Seeman, in *Proceedings of the US-CERN School on Particle Accelerators, Santa Margherita di Pula, Sardinia, 1985* (Ref. [1]), p. 121.

[3] See, for example, S. Myers, in *Proceedings of the US-CERN School on Particle Accelerators, Santa Margherita di Pula, Sardinia, 1985* (Ref. [1]), p. 176.

[4] K. Hirata, H. Moshammer, and F. Ruggiero, Part. Accel. **40**, 205 (1993).

[5] M. A. Furman, SLAC Report No. SLAC-AP-119, LBNL Report No. LBNL-42669, 1999.
[6] S. Krishnagopal and R. Siemann, Phys. Rev. Lett. **67**, 2461 (1991).
[7] S. Krishnagopal, Phys. Rev. Lett. **76**, 235 (1996).
[8] J. K. Koga and T. Tajima, Phys. Rev. Lett. **72**, 2025 (1994); J. Comput. Phys. **116**, 314–329 (1995); in *Accelerator Physics at the Superconducting Super Collider,* edited by Y. T. Yan, J. P. Naples, and M. J. Syphers, AIP Conf. Proc. No. 326 (AIP, New York, 1995), p. 215.
[9] E. B. Anderson, T. I. Banks, and J. T. Rogers, in *Proceedings of the Particle Accelerator Conference, New York, 1999* (IEEE, Piscataway, NJ, 1999).
[10] K. Ohmi, in *Proceedings of the International Workshop on Performance Improvement of Electron-Positron Collider Particle Factories* (KEK, Tsukuba, 1999).
[11] SLAC Conceptual Design Report No. SLAC-418, 1993.
[12] T. Tajima, *Computational Plasma Physics* (Addison-Wesley, Reading, MA, 1989).
[13] J. D. Jackson, *Classical Electrodynamics* (Wiley, New York, 1962), Chap. 1.
[14] R. W. Hockney and J. W. Eastwood, *Computer Simulation Using Particles* (IOP, Bristol, Philadelphia, 1988), Chap. 5.
[15] J. P. Christiansen and R. W. Hockney, Comput. Phys. Commun. **2**, 139–155 (1971).
[16] K. Hirata and F. Ruggiero, CERN LEP Note No. 661, 1988.
[17] M. Bassetti and G. Erskine, Report No. CERN ISR TH/80-06, 1980.
[18] Y. Nosochkov *et al.,* Report No. SLAC-PUB-8481, 2000.
[19] M. Izawa, Y. Sato, and T. Toyomasu, Phys. Rev. Lett. **74**, 5044 (1995).
[20] S. Krishnagopal, Phys. Rev. ST Accel. Beams **3**, 024401 (2000).